Fluorescence correlation spectroscopy for single-polymer diffusion in crowding solution

Ishihara Hironori

Index

Chapter 1：Introduction

1.1. Single-polymer diffusion

The morphology of synthetic polymers in solution changes depending upon the circumstance such as solvent and temperature. Diffusion process of polymers is one of the important research fields in polymer physics. Recent work in the field of single polymer dynamics has pushed into semi-dilute and semi-condensed polymer solutions. To detect the single-polymer diffusion under a condensed polymer condition, the fluorescent label is the powerful solution. By labeling a small number of polymers, we can use them as a tracer migrating in the media containing a large number of unlabeled polymers. In this way, the influence of intermolecular interactions on the single-polymer diffusion can be evaluated in semi-condensed polymer solutions. This approach makes it possible to uncover precise roles of hydrodynamic interactions in the migration of DNA.[1]

The detection of synthetic polymers in crowding solutions has attracted keen interest in biomedical applications.[2] It has been considered that the first event after an artificial material is inserted into a living body is the interaction with proteins. If the protein and the synthetic polymer form an association, the diffusion of synthetic polymers will change. In the last few years, the use of polymeric molecules as surface modifiers has been shown to be a very promising way to manipulate the surfaces – proteins interactions. The proper tuning of these interactions will hopefully lead us to the rational design of a modified surface that will improve biocompatibility.[3] To investigate a single-polymer and proteins in crowding solutions, therefore, will bring an insight into the origin of the biocompatibility.

One of the commonly used techniques for polymer diffusion is dynamic light scattering (DLS), which is a family of photon correlation spectroscopy (PCS). DLS has often been employed to measure the particle size of colloidal, submicron-size particles. When submicron-size particles are dispersed in solution and their sedimentation is negligible, the fluctuation of scattered light is the result of the Brownian motion of particles. If the scattering contrast of a particle is enough high, the constituents

can be organic, inorganic, or any mixture of them. Therefore, DLS becomes a powerful tool for monitoring the diffusion dynamics in a colloidal suspension. This versatility, however, makes it difficult to measure a target in a crowding circumstance because DLS detect signals from all scatterers. Moreover, it is difficult to observe the scattered light of small particles when large particles coexist because the scattering intensity is much emphasized for a large particle.

1.2. Photon correlation spectroscopy

DLS is one the most common techniques within the family of photon correlation spectroscopy (PCS). In PCS, we focus on the fluctuation of light scattered or emitted from the target. DLS exploits two properties common ro colloids, i.e., the Tyndall effect (scattering) and Brownian motion. Among other things, the scattered light intensity from colloidal suspension depends on the scattering angle (θ) and the observation time (t). These fact leads to the development of two types of scattering experiments: the static light scattering (SLS) , which measure the time averaged scattering intensity at various scattering angles and the DLS, which measure the time dependence of the intensity. In particular, DLS can measure particles much smaller than the wavelength of light. The time dependence of the scattering intensity arises from the fact that, under ambient conditions, colloidal particles are no longer stationary in suspension medium, rather they are moving in a random walk fashion by the Brownian motion process. When coherent monochromatic radiation is incident on a collection of particles, each particle acts as a secondary light source by scattering the radiation. Since particles are moving randomly in space, the distance traveled by the scattered wave from the particle to the detector varies with time. The net intensity fluctuates randomly in time as the relative position of the particles changes due to interference from the scattered waves from the particles. This causes random speckles which appear as fluctuating dark or bright spots in a detector. In order to observe such speckles, it is necessary to have a high spatial resolution of the photodetector and to measure these fluctuations

overtime. The area (or size) of a single speckle, known as the "coherence region" (A_{coh}) , depends on λ and the distance between the scatterer and detector (r) and is given by the following relation [4]

$$A_{coh} = \frac{\lambda^2 r^2}{\pi x^2}$$

where x is the radius of the scattering volume. The resolution of the measurement depends on the spatial coherence coefficient, which is determined by the ratio of the aperture area of the photodetector to the coherence area (A_{coh}). Therefore, in order to observe the random fluctuations in the signal with DLS, it is necessary to use appropriate pin holes (aperture) in front of the detector.

DLS measures the characteristic time of fluctuations of the scattered intensity, which depends on the diffusion coefficient of the particles undergoing Brownian motion. Because small particles diffuse relatively rapidly in the medium, the intensity signal fluctuates more rapidly than larger particles, which diffuse more slowly. Quantitative information about the time scale of this fluctuation in the scattering intensity is obtained by a signal processing technique known as autocorrelation. To understand the autocorrelation of scattering intensity, consider a time varying signal, $I(t)$ monitored at different time intervals. If we represent the scattered intensity at any time as $I(t)$ and those after a delay time τ as $I(t + \tau)$, the normalized autocorrelation function $g^2(\tau)$ of the scattered intensity can be written as

$$g^2(\tau) = \frac{\langle I(t)I(t+\tau)\rangle}{\langle I(t)\rangle^2}$$

It can be seen that when the delay time τ is zero, the signals are perfectly correlated and the numerator of the equation (unnormalized correlation function) yields the value $\langle I^2\rangle$, and when τ is infinite, the signals are perfectly uncorrelated and yielding a value of $\langle I\rangle^2$. From statistics, one can see that $\langle I^2\rangle$ is greater than or equal to $\langle I\rangle^2$.

Figure 1 shows a schematic representation of the fluctuations in intensity of particles of the fluctuations in the intensity of particles of two different size and the corresponding correlation functions. Note that the fast fluctuating signal decays faster than the correlation function obtained from the slow fluctuations.

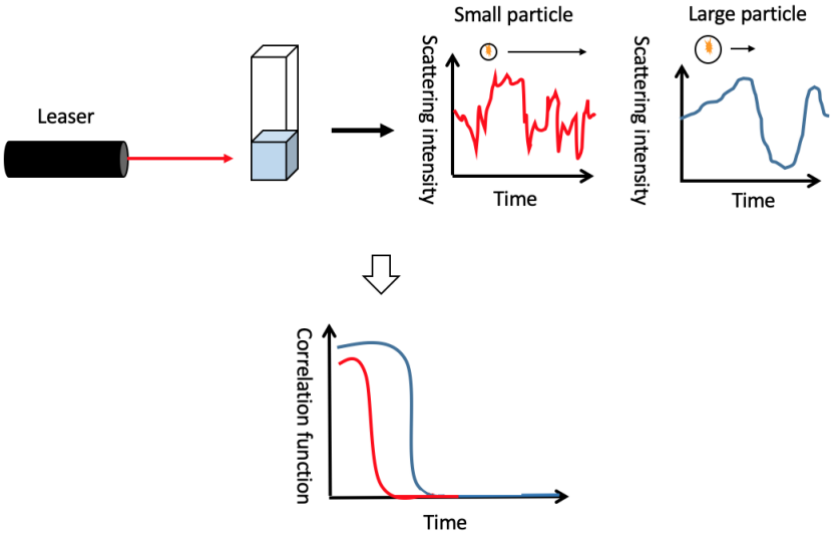

Fig.1 Principle of the PCS measurement

The essence of this method is to obtain particle size information by analyzing the correlation function. For a suspension of monodisperse spherical particles undergoes Brownian diffusion, the autocorrelation function decays exponentially with the delay time τ and is given by

$$g^1(\tau) = A \cdot e^{-Dq^2\tau} + B$$

where A is the amplitude of the correlation function, which depends on the aforementioned spatial coherence coefficient, B is the baseline, D is the translational diffusion coefficient of the particles, and q is the magnitude of the scattering vector expressed as $(4\pi n/\lambda)\ \sin(\theta/2)$. Where n is the refractive index of the medium. For spherical particles, the hydrodynamic radius R_h can be obtained from the

translational diffusion coefficient (D) using the Stokes－Einstein relationship.

$$D = kT/(6\pi\eta R_h)$$

where k is the Boltzmann's constant, η is the solvent viscosity, and T is the absolute temperature. If the particle is nonspherical, then R_h is often taken as the apparent hydrodynamic radius or equivalent sphere radius. This is how the particle size information is arrived in a typical DLS experiment.

Thus, since DLS can easily measure particle size, a variety of materials have been measured, including synthetic polymers, biopolymers, and inorganic materials. In particular, it should be noted that the ability to measure the particle size of ceramics.

Among them, High-entropy oxides (HEOs), as multi-component ceramics with high configurational entropy, have been of recent interest due to their attractive properties including photocatalytic activity for H_2 production and CO_2 conversion. It is difficult to determine the average particle size of multicomponent ceramics due to the large number of components. This paper is an example of a solution to that problem.[5]

Although DLS has been used as a useful tool to understand the dynamics of all kinds of materials, it is difficult to accurately understand the dynamics of complex systems, such as crowding solution, agglomerate in vivo systems, and when large particles are present.

1.3 Fluorescence correlation spectroscopy

Fluorescence correlation spectroscopy (FCS) is also categorized into PCS family, which detects only the fluctuation of the fluorescent intensity emitted from the target. The largest difference between DLS and FCS is the selectivity of the diffusant. FCS was first introduced as an analytical technique applied for chemical dynamics of DNA–drug intercalation by Magde, Elson, and Webb in the early 1970s.[6] However, due to poor signal-to-noise ratios, this technique did not become extensively used.

By combining with confocal optics, the low detection efficiency is overcome. The confocal optics is very effective to suppress the background fluorescent emission and to detect the fluctuation of chromophores in a quite limited volume a few nano-little.

Other important developments are related to the stability of the advent of laser light sources, the availability of photodetectors with high sensitivity, and the introduction of new microscope techniques. The development of FCS has been linked to the use of optical microscopes for two reasons. First, the microscope is a very efficient optical instrument. High numerical aperture (NA) objectives capture a significant fraction of the fluorescent light that is emitted randomly in all spatial directions. Second, the microscope optics allows the generation of very small observation volumes. High NA objective focuses the incident laser beam to a diffraction-limited spot size. Nowadays, in view of the advantages of high spatial and temporal resolution, short analysis time, and low sample consumption, FCS has gradually developed as a technique for the study of chemical kinetics, conformation dynamics, and molecular diffusion in solution and on membranes.[7]

To employ FCS, however, we must get over the fluorescence labeling of a target.

When performing the synthesis, we can select an appropriate monomer that contains both the polymerizable group and the chromophore.

FCS was employed to observe the dynamics of the denaturation of deoxyribonucleic acid (DNA).[8] Here, the fluctuation of ethidium bromide (EtBr) at thermodynamic equilibrium for attaching and detaching to DNA was monitored. Because EtBr inhibits nucleic acid synthesis, the denaturation of DNA is induced by the intercalation of the dye. EtBr attached to DNA strongly emits the fluorescence light, and then the fluctuation of the number of dyes at a small volume is correlated with the fluctuation of the fluorescent intensity.[9]

Contrary to the application in bioscience, FCS has been less employed to investigate the synthetic polymer solution. One of the pioneer works has been reported by Dominique et al.[10] For example, in

this review reported diffusion of small molecular probes and nanoparticles in covalently crosslinked polymer gels. Diffusion in gels is a complex phenomenon affected by several factors, such as the mesh size of the gel, its microstructure, the degree of swelling, the size of the diffusing species, and interactions between diffusing species and gel. Michelman-Ribeiro reported on the diffusion of 5-carboxytetramethylrhodamine (TAMRA) in poly(vinyl alcohol) (PVA) solutions and gels prepared at various polymer concentrations and crosslink densities.[11] The authors found a simple linear relation between the difference of diffusion times [s(gel)-s(solution)] of the probe in the gel and the non-crosslinked polymer solution and the elastic modulus of the same gel, indicating that diffusion of the probe particles is strongly correlated with the gel elasticity.

1.4 FCS for crowding solution

Recently, the demand to observe the diffusion behavior of a synthetic polymer in molecularly crowding systems such as biological environments has rapidly increased. A significant progress has been attained in the field of drug delivery devices. Many of the new drug delivery devices are polymeric. Particularly, Molecularly imprinted polymers (MIPs) are the class of new synthetic polymeric materials that provide a high selectivity towards the selected molecules. [12] They offer high thermal, chemical and mechanical stabilities. Those advantages caused broad applications in the analytical chemistry, where they are used for the separation or detection of many compounds.[13] Molecular imprinting technology has a high potential for the preparation of optimized drug delivery forms. Here, molecularly imprinted polymers (MIPs) are promising new materials for such purposes, but their application in this field is nowadays at a developing stage.

If we could label the target with a fluorescent chromophore, FCS enables us to monitor the diffusion even in a crowding solution, since FCS detects only the fluctuation of the fluorescent light. This thesis shows the application of FCS for monitoring a single-polymer diffusion in a crowding solution. The aqueous solution of poly(*N*-isopropylacrylamide) (PNiPAm) is selected as the test case, where phase separation occurs by heat. In the vicinity of the phase separation, the polymers gather toward a macroscopic phase change. DLS cannot monitor the single-polymer diffusion in this process because of the large contrast between the aggregate and the unimer.

Chapter 2：Setup of fluorescence correlation spectroscopy

2.1 Optical configuration

In the following, the basic principles of FCS will be summarized. In a typical FCS experiment, as shown in Figure 2, a collimated laser beam is focused by an objective lens into a diffraction limited confocal volume within the sample placed on a glass coverslip.

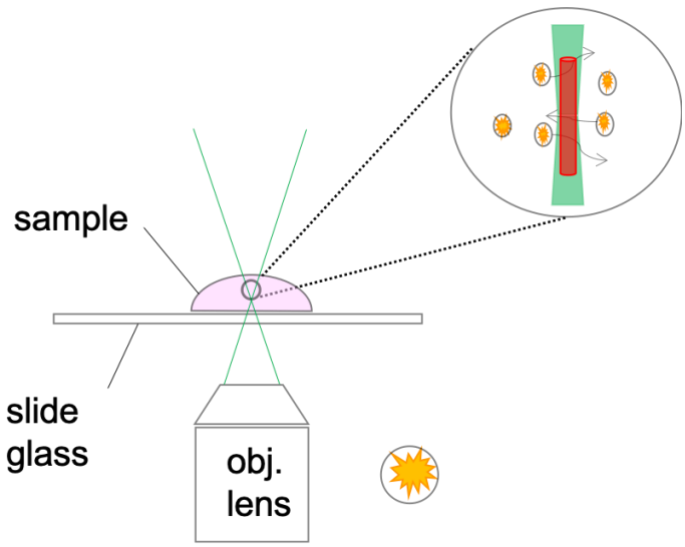

Figure 2. Schematic image of FCS measurement.

In FCS, one monitors the fluorescence fluctuation of a tiny observation volume, where fluorescently labeled molecules may migrate in and out by Brownian motion . For a larger molecule, the fluctuation of the fluorescence intensity becomes slow, and then the auto-correlation function decays with a longer correlation time (Figure 3). The correlation time, therefore, reflects the size of the target or the micro-viscosity around the target. In this case, what is actually observed is the diffusion coefficient of the molecule. On the other hand, it is also possible to estimate the "number of molecules" by looking at the "fluctuation rate" of the fluorescence intensity.

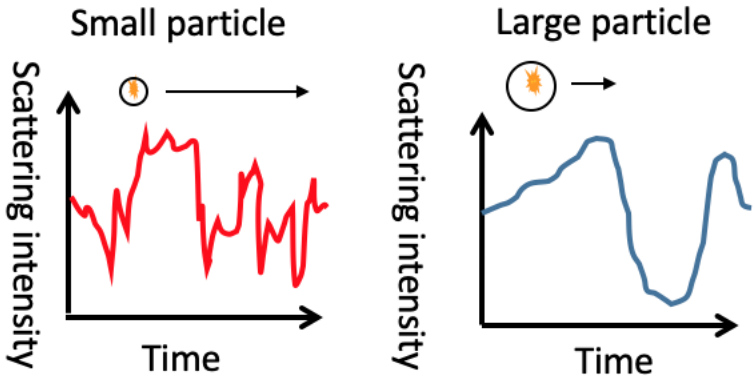

Figure 3. Schematic image of the relationship between the intensity fluctuation of fluorescence and particle size of diffusants.

Analysis by Correlation Function

In FCS, we consider that the temporal fluctuation of the light, $I(t)$, which is either scattered or emitted, is associated with the diffusive motion of particles. The second-order autocorrelation function $C(\tau)$ is calculated with,

$$C(\tau) = \langle I(t)I(t+\tau)\rangle \tag{1}$$

where <> indicates the temporal average and t is the lag time. If the light intensity during the measurement is represented as $\langle I\rangle$ and the deviation from the $\langle I\rangle$ at t is expressed by $I(t) = \delta I(t) + \langle I\rangle$, the equation (1) can be transformed as follows.

$$C(\tau) = \langle \delta I(t) + \langle I\rangle\rangle\langle \delta I(t+\tau) + \langle I\rangle\rangle$$

And it gives

$$= \langle \delta I(t)\delta I(t+\tau)\rangle + \langle I\rangle\big(\delta I(t)\big) + \langle I\rangle\langle \delta I(t+\tau)\rangle + \langle I\rangle^2$$

where $\langle \delta I(t)\rangle$ and $\langle \delta I(t+\tau)\rangle$ are both the mean (i.e., deviation) of the fluctuations relative to the

mean intensities, and thus both values should be zero. As a result, we obtain

$$C(\tau) = \langle \delta I(t) \delta I(t+\tau) \rangle + \langle I \rangle^2 \tag{2}$$

This equation consists of the square of the mean intensity $\langle I \rangle^2$ and a time-dependent term $\langle \delta I(t) \delta I(t+\tau) \rangle$ (Figure 4a). Thus, the autocorrelation function plotted against τ can be divided into a stationary part and a time-dependent part as shown in Figure 4b.

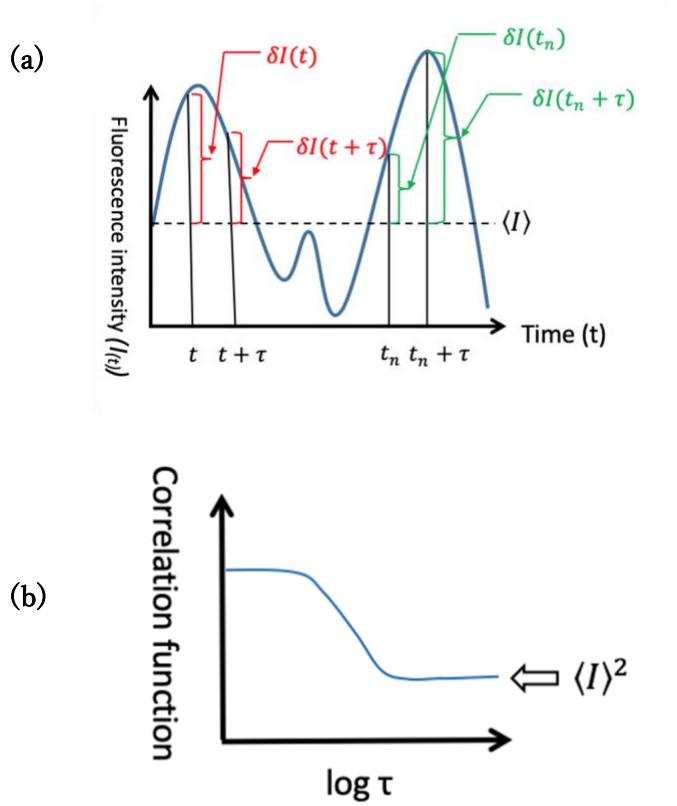

Figure 4 **(a)** Temporal variation of the light intensity due to the number fluctuation. **(b)** Schematic illustration of $C(\tau)$. The correlation of the light intensity disappears after a several period, and then the value reaches to $\langle I \rangle^2$.

To normalize $C(\tau)$, the equation (2) is divided by $\langle I \rangle^2$, resulting in

$$C(\tau)/< I >^2 = G(\tau) = 1 + \frac{\langle \delta I(t) \delta I(t+\tau) \rangle}{<I>^2} \quad (3)$$

At $\tau = 0$, we obtain

$$G(0) = 1 + \frac{\langle \delta I(t) \delta I(t+0) \rangle}{I^2} = 1 + \frac{\langle \left(\delta I(t)\right)^2 \rangle}{\langle I \rangle^2} \quad (4)$$

In the case of FCS, the fluorescence intensity is proportional to the number of dyes N, $I \propto N$. Thus, the equation (4) can be written by the number fluctuation as follows.

$$G(0) = 1 + \frac{\langle \left(\delta N(t)\right)^2 \rangle}{\langle N \rangle^2} \quad (5)$$

$\langle \left(\delta N(t)\right)^2 \rangle$ is the variance (the square means of the standard deviations). In the case that the diffusive motion of each fluorescent dye is independent and the motion is based on the random walk, the number of fluorescent dyes in the observation field follows a Poisson distribution. In a Poisson distribution, the mean quantity and the variance are equal.

$$\langle \left(\delta N(t)\right)^2 \rangle = \langle N \rangle$$

Thus,

$$G(0) = 1 + \frac{1}{N} \quad (6)$$

The relationship between $G(0)$ and the translational diffusion for FCS was derived by Rigler and co-workers.[14] The observation field is assumed to have a cylindrical shape along the optical axis, whose radius is w with the half-height of z. The probability that a fluorescence dye is found in the one

dimension of the observation field is proportional to $(1+\tau/\tau_D)^{0.5}$, where τ_D is the relaxation time caused by the diffusion of the dye. The normalized auto-correlation function $G(\tau)$ is expressed as

$$G(\tau) = 1 + \frac{1}{N}\left(\frac{1}{1+\tau/\tau_D}\right)\left(\frac{1}{1+(1/s)^2(\tau/\tau_D)}\right)^{\frac{1}{2}} \quad (7)$$

where s is the shape factor ($s = z/w$). The relationship between τ_D and the translational diffusion coefficient D is

$$D = w^2/4\tau_D \quad (8)$$

Using the relationship in Eq. (7), we obtain

$$g(\tau) = 1 + \frac{1}{N}\left(\frac{1}{1+4D\tau/w^2}\right)\left(\frac{1}{1+4D\tau/z^2}\right)^{\frac{1}{2}} \quad (9)$$

This is the fundamental expression of $G(\tau)$ used for the analysis of FCS signals.

FCS analysis

The FCS profiles were analyzed by the following fitting function,

$$G(t) = 1 + \frac{1}{<N>}\left\{f\left(\frac{1}{1+t/\tau_1}\right)\left(\frac{1}{1+(1/s)^2 t/\tau_1}\right)^{1/2} + (1-f)\left(\frac{1}{1+t/\tau_2}\right)\left(\frac{1}{1+(1/s)^2 t/\tau_2}\right)^{1/2}\right\} \quad (7)'$$

where $\tau_{D,n}$ (n = 1, 2) represents the relaxation time of diffusants, s is the aspect ratio of the confocal volume, $<N>$ is the average number of the fluorescent dye molecules in the confocal volume element, and f is the fraction of the first component. The radial and axial dimensions of the confocal volume are represented by w_r and w_z, respectively. D_n (n = 1, 2) of the fluorescent-labeled species can be calculated by τ_n as follows.

$$D_n = \frac{w_r^2}{4\tau_{D,n}} \qquad (10)$$

The hydrodynamic radius of the diffusants, R_h, was estimated by Stokes-Einstein relation with D_n.

Experimental setup

The FCS system was constructed based on a confocal laser optics system, and the optical scheme of the confocal laser optics system is shown in Figure 5. In the following, we describe the detailed experimental setup of the actual FCS device used.

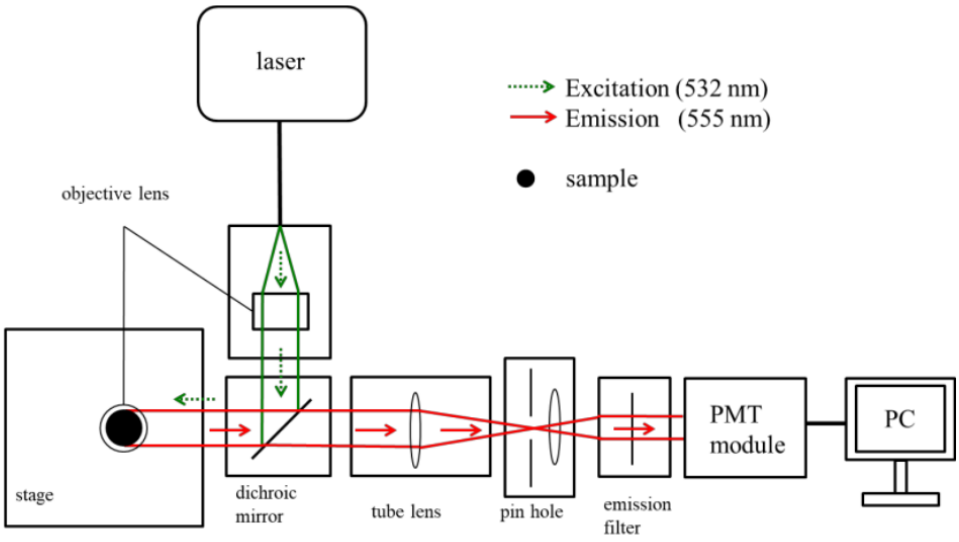

Figure.5　Setup drawings of FCS

Laser

The laser used to cause fluorescence excitation was a λ=532 nm YAG laser.

Beam Expander

Generally, a beam expander consists of a lens that serves to expand the diameter of the incident laser beam and two lenses that collimate the beam (collimated light) and emit it.

In this setup, a beam aligner block, HAMAMATSU PHOTO's A10760, is used.

The beam aligner block uses an objective lens with infinity correction to guide a laser beam or other light into an optical fiber cable with an FC connector and to extract the beam from the optical fiber cable as a collimated beam (Fig. 6). A cover is attached around the objective lens, and a cover is also attached to the outside of the block to improve light shielding.

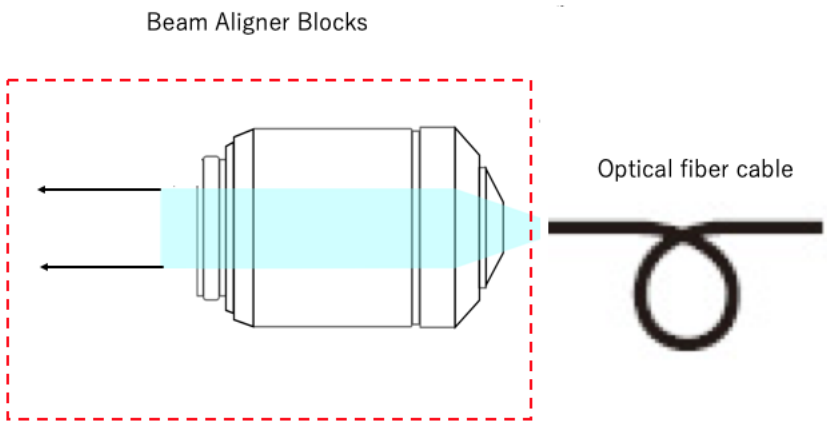

Fig.6　Example of collimator use in beam aligner block

Beam splitter block

A cube-shaped dichroic mirror can be incorporated to reflect certain wavelengths and transmit light in other wavelength regions by means of a multilayer of derivative materials with different refractive indices. In this system, HAMAMATSU PHOTO's A10035 is used, and the built-in dichroic mirror is Edmund's #86-334.

Objective Lenses

This system uses an OLYMPUS UAPON 40X340. Basic information such as the number of apertures and resolution is shown below.

Aperture of objective lens (NA)

A high numerical aperture objective lens is desirable. The numerical aperture NA is an important value that determines the resolution, depth of focus, and image brightness of an objective lens. The larger this value is, the higher the resolution and the shallower the depth of focus.

$$NA = n \cdot \sin\theta$$

n is the refractive index of the medium between the objective lens tip and the sample.

θ is the angle between the light ray passing through the outermost objective lens and the center of the lens (optical axis).θ is the angle between the ray passing through the outermost objective lens and the center of the lens (optical axis) (Figure 7). The numerical aperture of UAPON40X340 is NA = 1.15.

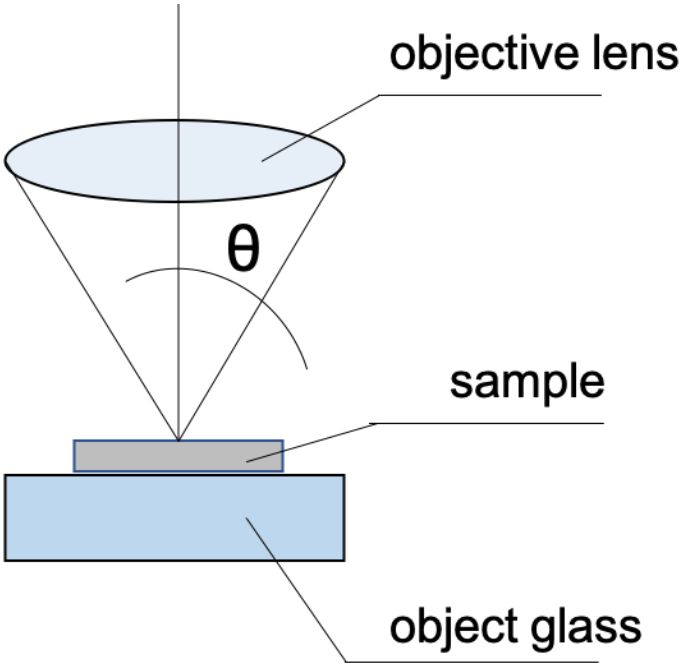

Fig.7　Definition and determination of the numerical apertures

Resolution

Resolution is the smallest interval at which it is possible to distinguish points or lines that are very slightly separated from each other. The resolution (D.L.) is determined by the aperture NA and wavelength λ.

$$D.L.(nm) = \frac{\lambda}{NA}$$

The aperture of UAPON40X340 is D.L. = 282 (nm).

Pupil Diameter of Objective Lens, Same Focal Length and Spot Diameter

The beam diameter emitted from the pupil of the objective lens is calculated by the focal length f of the objective lens and the numerical aperture NA as follows.

$$\text{Pupil Diameter } (\Phi_p) = 2 \times f \times NA$$

The distance from the body surface of the objective lens to the object surface when focused is called the same focal length. When a beam of light with a uniform intensity distribution is incident on an objective lens, the focused diameter is called the spot diameter. In the case of a light source with a Gaussian distribution in its cross-section, such as a laser beam, the laser beam diameter is generally expressed as a value equal to $1/e^2$ of the peak and can be calculated using the following formula.

$$\Phi_s = \frac{4\lambda f_{obj}}{\pi \Phi_p}$$

The outline of these lenses is shown in Figure.8. The UAPON40X340 has a pupil diameter of 10.35 nm, a focal length of 45 mm, and a spot diameter of 295 nm.

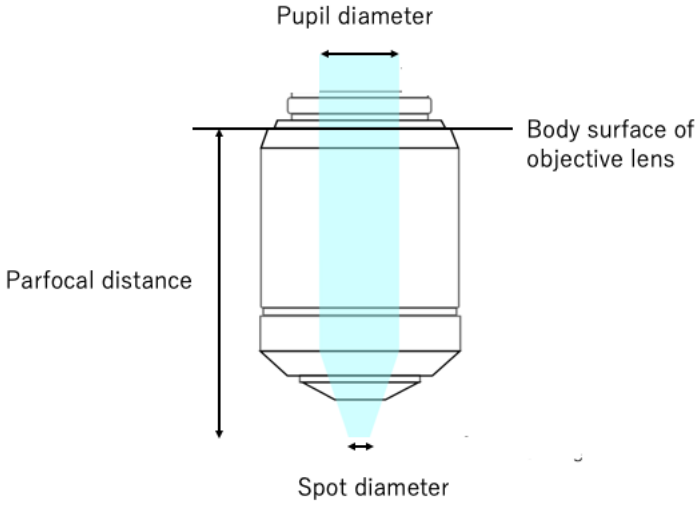

Figure.8　The outline of Pupil Diameter of Objective Lens, Same Focal Length and Spot Diameter.

Infinity-Corrected Optics and Magnification

An optical system that uses an objective lens and an imaging (tube) lens to create an image is called an infinity-corrected optical system (Fig. 9), which is used in this FCS optical system.

f1 is the focal length of the objective lens and f_2 is the focal length of the imaging (tube) lens. The magnification is determined by the ratio of the focal length of the objective lens and the focal length of the imaging lens.

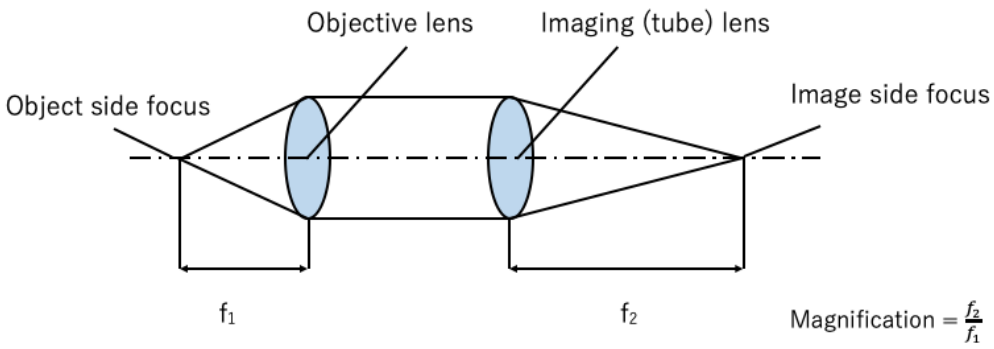

Fig.9　Schematic of infinity-corrected optics

Tube Lens Block

The light rays from the object pass through the infinite correction objective lens and enter the imaging lens as a collimated light beam. The imaging lens forms an image at the focal distance position. The tube lens block is a video lens for the infinity-corrected objective lens with a built-in imaging lens. In this system, HAMAMATSU PHOTO's A10859-01 is used.

Pinhole block

A holder block to which a mount-type pinhole is attached and whose position can be adjusted in the XY direction. The built-in lens makes the light passing through the pinhole parallel and guides it to the light detector. This system uses HAMAMATSU PHOTO's A11027.

Emission filter

An absorption filter is an optical element that separates fluorescence emitted from a sample from other unwanted scattered light. It transmits long-wavelength fluorescence transmitted through the dichroic mirror and does not transmit other light such as leakage light from excitation (scattered light from the sample and optical system).

In this system, Edmund's #49-027 is used.

Photomultiplier tube (PMT) module

PMT modules are used to detect faint optical signals from weak synchrotron radiation sources. Of importance here is the quantum efficiency, which is a parameter to be considered since it directly affects the counting rate of molecules. In this system, the detector is replaced by an avalanche photodiode (APD) (H10682-110, HAMAMATSU PHOTO).

The correlation function was constructed using a digital hardware collimator. Signals from the

detectors are correlated on-line and the autocorrelation function can be monitored in real time. The system uses the Flex02-12D/C digital correlator (correlator.com).

2.2 Diffusion of rhodamine 6G

Due to their photostability, their large extinction coefficients and high fluorescence quantum yield, rhodamine derivatives are widely used for diffusion measurements or as labels in environmental biochemical and interfacial studies. Among other uses, they are employed to calibrate FCS, a technique now widely employed to determine molecular sizes and to characterize translational (Brownian) diffusion in complex media. In this experiment, among the many Rhodamine derivatives, Rhodamine 6G is employed for determining experimentally s (=z/w) of (7)' (diffusion coefficient, D = 4.14 × 10^{10} m^2 s^{-1} at 25 °C) was used. [15]

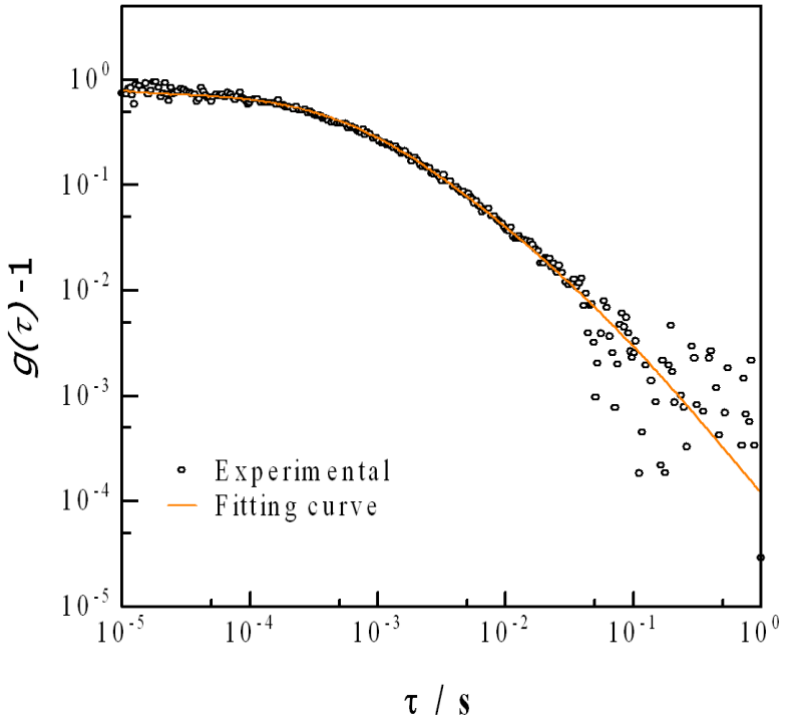

Figure 10. Fitting results of the FCS signal for Rhodamine 6G

Figure 10 shows the fitting results of the FCS signal for Rhodamine 6G. The value of *s* obtained from this fitting was 4.0×10^{-2}.

2.3 Fluorescence-labeled polymer under an extremely diluted condition

FCS measurements can observe diffusion behavior in extremely diluted conditions that could not be measured by DLS. Figure 11 shows the fitting result of the FCS signal when the solution concentration is $2.0 \times 10^{-5}\ wt\%$. Such dilute concentrations, aggregation does not occur even at temperatures where would normally occur. Although we will not discuss much in this paper, we will observe diffusion behavior under these conditions in the future.

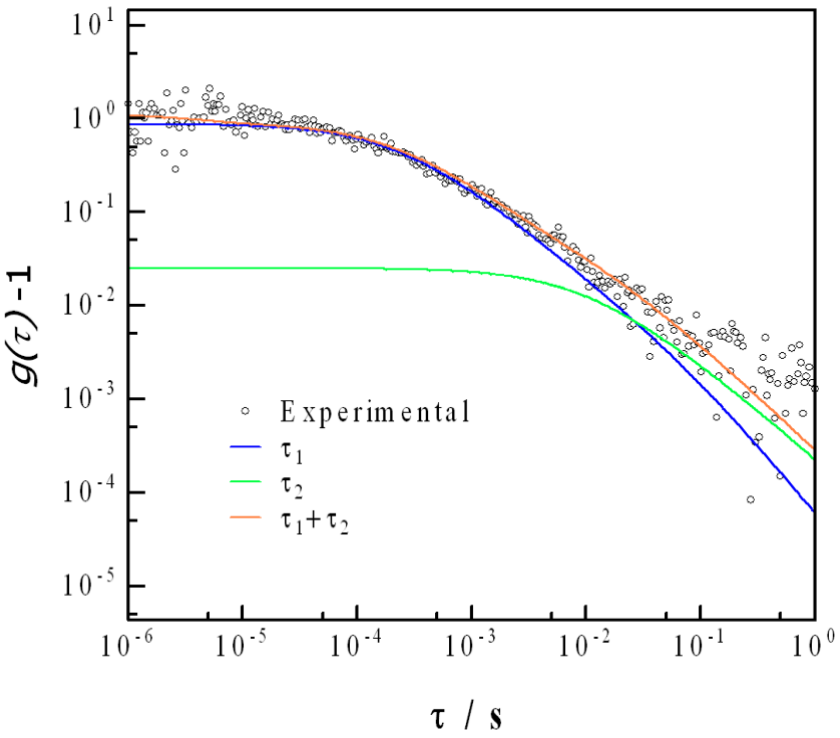

Figure 11. Fitting results of the FCS signal for P(NiPAm-co-RhB) i-52r in water at $2.0 \times 10^{-5}\ wt\%$

Chapter 3: Single-polymer diffusion in the aqueous solution of Poly(N-isopropylacrylamide)

3.1. Introduction

Liquid-liquid phase separation (LLPS) has a long history of research in the field of physical chemistry, but it has recently come into the spotlight again in the field of molecular cell biology. Phasing biology is a new field of life science,[16] which focuses on the droplets formed by LLPS with biomacromolecules and their role in various biological phenomena, including gene transcription and translation, protein folding, signal transduction, and intracellular quality control.[17] Because the droplets formed through the intracellular LLPS are mainly composed of biomacromolecules such as proteins and RNAs,[18] we expect that the fundamental aspects are understandable based upon polymer science.

The intracellular LLPS is induced by a protein containing intrinsically disordered regions (IDRs), which will not form any defined three-dimensional structure. The interaction between IDRs involves multiple modes such as hydrophobic,[19,20] hydrogen bonding (more generally dipole-dipole),[20,21] electrostatic,[22] and π -orbital interactions.[20,23] These interactions also play a fundamental role in the protein complexes formed by protein-protein binding.[24] An important character of the droplets in phasing biology is liquidity because the generation and collapse of these droplets should be induced by a small perturbation in living cells.

One of the large differences between LLPS with a general synthetic polymer and an intracellular LLPS lies in the size of droplets. The size of the intracellular droplets does not increase beyond a few micrometers. In many cases of LLPS with a synthetic polymers, on the

other hand, the size of droplets does not stop growing until the total interface area becomes minimum, and then the interface becomes visible to the eyes. The latter is often referred to as a macroscopic LLPS. For the biological intracellular LLPS, there must be a mechanism that stabilizes the submicron-size droplet. The key may be found in an aqueous solution of poly(N-isopropyl acrylamide) (PNiPAm), which shows curious behaviors in the phase separation. In general, a solution of synthetic polymers undergoes macroscopic LLPS such as poly(N,N-diethylacrylamide) (PNdEAm) /water [25] and poly[2-(2-ethoxy)ethoxyethyl vinyl ether] / water [26] systems. At equilibrium of the macroscopic LLPS, two liquid phases are visually observed. For PNiPAm/water system, on the other hand, the opaque solution above the cloud point (Tc) temperature cannot separate into two transparent liquid phases.[27] Several researcher groups have pointed out that small droplets formed above Tc are stable and do not increase their size by further heating.[28-31]

The comparison between the phase behavior of the aqueous solutions of PNiPAm and PNdEAm is quite interesting. Tc of the 1-2 wt% aqueous solution of atactic PNdEAm and PNiPAm is almost the same,[32,33] and the salt effect on Tc of the aqueous solutions resembles.[24,35] However, their phase behaviors are different in some points. The effects of cosolvent are different for the two polymers; the co-nonsolvency is found for PNiPAm in water-methanol mixtures while it is not for PNdEAm.[36,37] The tacticity (stereoregularity) effects on the solution properties of these two polymers are opposite;[32,33] Tc of PNiPAm in water decreases with increasing meso diad content (m), while that of PNdEAm increases. The endothermic peak in the differential scanning calorimetry for PNdEAm in water is much broader than that for PNiPAm in water.[37] The aqueous solution of PNiPAm shows a hysteresis in demixing and mixing processes, while that of PNdEAm does not.[38] These differences are possibly concerned with the fact that PNiPAm can form a C=O···H－N intra- and

intermolecular hydrogen bond among the amide groups. [39-41]

In this report, we investigate how the dehydration of PNiPAm upon heating is different from that of PNdEAm by using the fluorescent probe method. As several researchers have indicated, the macroscopic LLPS is inhibited for the PNiPAm/water system.[39,42] That is, the dehydration of polymers does not always induce macroscopic LLPS of the aqueous solutions. However, it is quite difficult to discuss this subject because the dehydration temperature and Tc for an atactic PNiPAm are very close. In the previous paper,[43,44] on the other hand, we have revealed that a concentrated aqueous solution of m-rich PNiPAm forms a transparent physical gel much below Tc. This implies that the dehydration of m-rich PNiPAm occurs antecedently before the system undergoes macroscopic LLPS. In a dilute region, it is expected that the dehydrated polymer chains form nanodroplets, which may resist the coalescence toward macroscopic LLPS.

3.2. Experimental

Fluorescent probe comonomer.

Acryloxyethyl thiocarbamoyl rhodamine B (RhB) was purchased from Merck and used as received. *N*-[2-[[[5-(dimethylamino)-1-naphthalenyl]sulfonyl]amino]ethyl]-2-propenamide (DAN) was prepared by the method found elsewhere.[45,46] In brief, a THF solution of dansyl chloride (0.15 L, 4.6 $\times 10^{-2}$ mol L^{-1}) was added dropwise to a THF solution of ethylenediamine (0.30 L, 2.3 $\times 10^{-1}$ mol L^{-1}) at 0 ° C. The mixture was stirred at 0 ° C for 3 h, followed by the addition of an aqueous solution of KOH (2.0 $\times 10^{-2}$ L, 1.0 mol L^{-1}). After THF was evaporated, the aqueous layer was extracted with CH_2Cl_2 (4 × 0.10 L). $MgSO_4$ was used for drying the combined organics, and then CH_2Cl_2 was evaporated to leave an oil with a pale yellow-green color. By crystallization from benzene/hexane, *N*-dansyl ethylenediamine (**1**) was obtained as light green needles. Acryloyl chloride was added to a molar equivalent amount of **1** and triethylamine in THF at room temperature. After stirring overnight, the solid salts were removed by filtration. DAN was purified by column chromatography on silica gel with diethyl ether/hexane (4/1) as eluent. The chemical structure of RhB and DAN are shown in Figure 12.

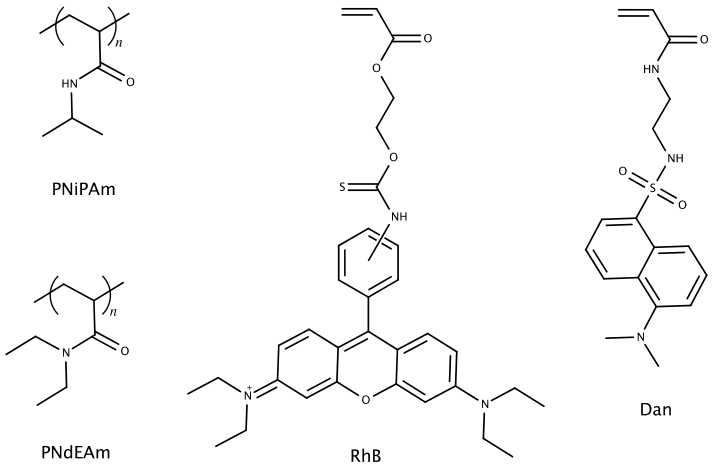

Figure 12. Chemical structures of PNiPAm, PNdEAm, RhB, and Dan.

Fluorescence-labeled stereo-controlled PNiPAm and PNdEAm.

Fluorescence-labeled PNiPAm and PNdEAm with various meso diad (*m*) contents were synthesized. Chemical structures of PNiPAm and PNdEAm homopolymers are shown in Figure 1. The molecular weight and the tacticity of polymers are controlled by reversible addition-fragmentation chain transfer (RAFT) polymerization with a Lewis acid catalyst.[47-49] α,α-Azobisisobutyronitrile (AIBN, Wako) and *N*-isopropylacrylamide (NiPAm, Wako) were recrystallized from a benzene/hexane solution. *N,N*-diethylacrylamide (NdEAm) was purified by vacuum distillation. 1-Phenylethyl phenyldithioacetate (PEPD) was used for PNiPAm and *N,N*-diethyl-s-thiobenzoylthiopropionamide (DETP) was used for PNdEAm as the RAFT agent. The molar ratio of DAN or RhB to the monomer in preparation is 1×10^{-3}. The polymer products were recovered by freeze-drying after dialysis to water. The number-averaged molecular weight (M_n) and polydispersity (M_w/M_n) of the prepared samples were determined by size exclusion chromatography (SEC; Intelligent HPLC system) made by JASCO (Tokyo, Japan) equipped with SB-807 HQ (Shodex) guard column, two linear poly(hydroxy methacrylate) beads columns (Shodex SB-802.5 HQ and SB-806M), and a RI-2031 differential refractive-index detector. The eluent was *N,N*-dimethylformamide (LiBr 10 mM) at 60 °C with a flow rate of 0.35 mL min^{-1}. SEC chromatogram was calibrated by using a series of standard polystyrene samples (Shodex, SM-105). ^{1}H NMR spectra were recorded on a JEOL (Tokyo, Japan) JNM-LAMBDA spectrometer (500 MHz). The tacticity of the samples was represented by the *m* content, which was determined from the methylene proton peaks of the polymer measured in DMSO-d_6 at 145 °C.[33,48] The M_n, M_w/M_n, and *m* were listed in Table 1.

Table 1. M_n, M_w/M_n, and m of polymers

Sample ID	m	M_n / g mol^{-1}	M_w/M_n
P(NiPAm-co-Dan)			
i-46f	46	3.9×10^4	1.3
i-49f	49	4.9×10^4	1.4
i-52f	52	5.1×10^4	1.4
i-56f	56	5.3×10^4	1.3
i-58f	58	5.1×10^4	1.4
PNiPAm			
i-52	52	3.7×10^4	1.2
P(NiPAm-co-RhB)			
i-52r	52	3.9×10^4	1.4
P(NdEAm-co-DAN)			
e-56f	56	2.6×10^4	1.4
e-70f	70	3.5×10^4	1.6
e-90f	90	7.0×10^4	1.3

[NiPAm] = 2.23 M, [NdEAm] = 2.23 M, [AIBN] = 0.8 mM, [PEPD] = 8.94 mM in methanol/toluene(1/1, v/v) mixture. Polymerization at 60 °C.

Turbidimetry and steady-state fluorescence spectroscopy.

The temperature dependence of transmittance of 650 nm light, $\Phi(T)$, was monitored using an apparatus equipped with a Si photodiode detector (Hamamatsu Photonics). The temperature was controlled by a homemade thermostat with an accuracy of 0.1 °C. The heating rate was less than 0.2 °C min^{-1}. Steady-state fluorescence spectra were recorded by a Hitachi F-2500 spectrometer with an excitation wavelength of 340 nm. The voltage of the photomultiplier was 700 V and the scan speed was 300 nm/min. The labeled polymer solutions were placed in 10 mm quartz cells and the temperature was controlled by a homemade thermostat with an accuracy of 0.1 °C. At each temperature, the fluorescence spectrum was recorded 10 min after the temperature becomes stable.

The representative fluorescence emission spectra of P(NiPAm-co-DAN) and P(NdEAm-co-DAN) are shown in Figure S1 in the supporting information (SI). The mean center of the fluorescence emission envelope (λ_m) reflects the micropolarity in the vicinity of the probe. Figure S2 in SI shows the change in λ_m of DAN monomer in water/methanol and water/1.4-dioxane (ε_r= 2.25) mixture. The dielectric constant ε_r of water, methanol, and 1.4-dioxane are 80.1, 32.7, and 2.25, respectively. λ_m is 525 nm in methanol, but 560 nm in water. λ_m shifts monotonically with varying the solvent composition in the mixture. Asano et al. have revealed that the wavelength of maximum emission of an atactic P(NiPAm-co-DAN) ($m \sim 46$) exhibits a linear correlation with the polarity in the vicinity of the probe.[46]

Fluorescence Correlation Spectroscopy (FCS).

FCS measurement was carried out by a homemade apparatus with a confocal optical setup with a cross correlation arrangement. More information can be found in Section 1.

3.3. Results and Discussion

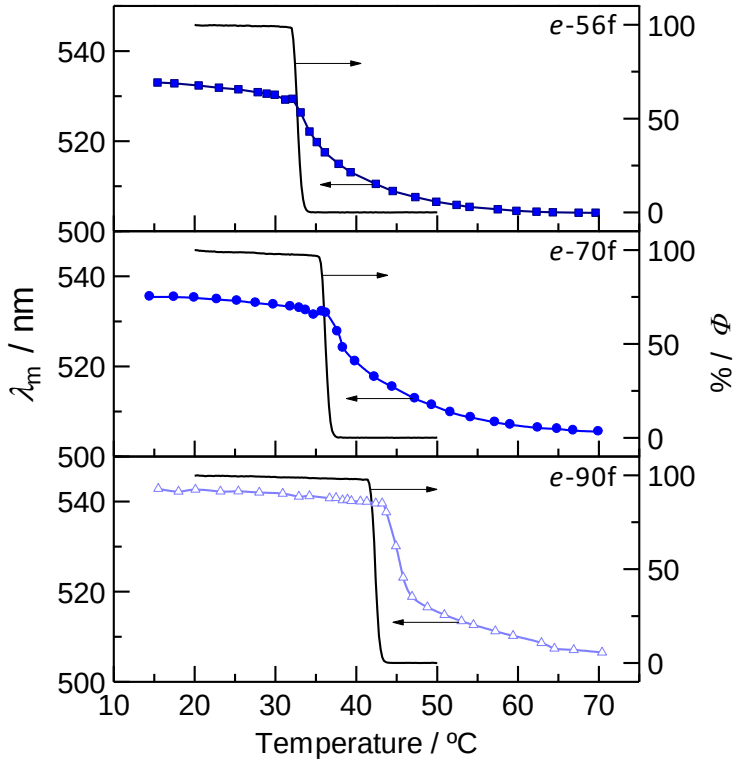

Figure 13. Comparison between $\lambda_m(T)$ and $\Phi(T)$ for the stereo-controlled P(NdEAm-co-DAN)s in water at 0.1 wt%.

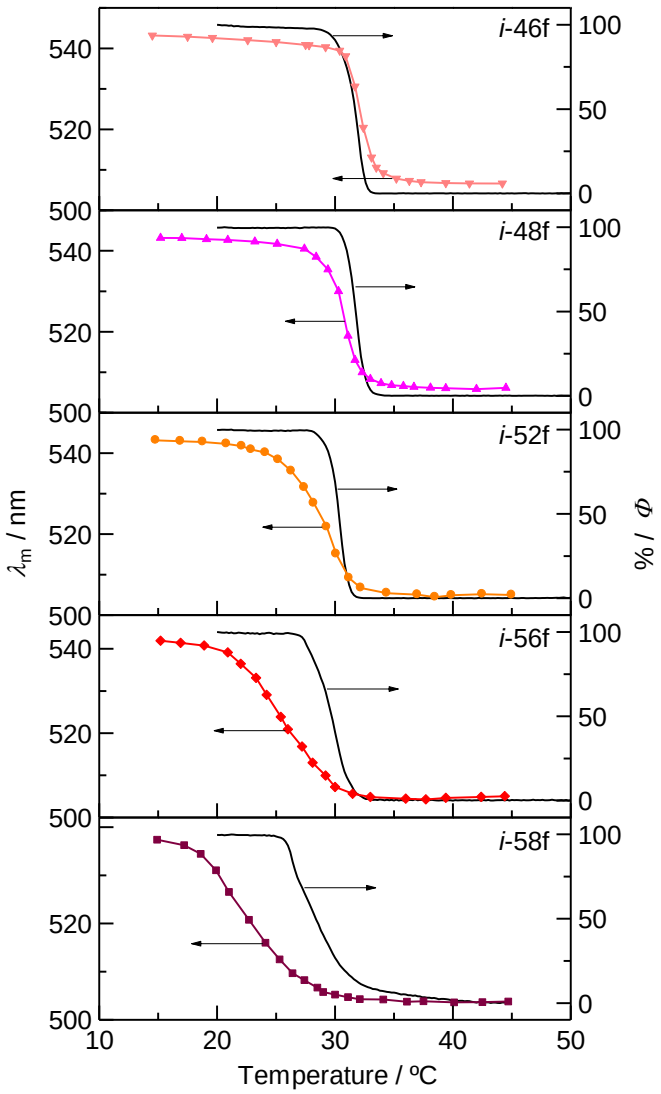

Figure 14. Comparison between $\lambda_m(T)$ and $\Phi(T)$ for the stereo-controlled P(NiPAm-co-DAN) in water at 0.1 wt%.

Comparison between the thermal change in the fluorescence and transmittance.

Figures 13 and 14 show the temperature dependence of λ_m and Φ for the stereo-controlled P(NdEAm-co-DAN)s and P(NiPAm-co-DAN)s in water at 0.1 wt%, respectively. λ_m gradually decreases with increasing temperature, and then the curvature changes toward a greater rate of decrease at a certain point. The decrease in λ_m indicates that the circumstance of DAN becomes hydrophobic. $\Phi(T)$ seems to be correlated with $\lambda_m(T)$; $\lambda_m(T)$ may reflect the change in the hydration state of polymer chains

associated with the phase change. For PNdEAm *e*-56f, λ_m decreases from ca. 530 nm to below 510 nm with increasing *T*, indicating that the micropolarity around PNdEAm chains goes down to below ε_r=10 when the polymer chains are fully dehydrated (the relationship between λ_m and ε_r can be found in Figure S2).

The decrease in Φ for the aqueous solution of PNiPAm and PNdEAm is caused by the formation of micron size droplets corresponding to the phase separation.[38] In this paper, the onset temperature of the abrupt drop in $\Phi(T)$ is referred to as T_c. By carefully investigating the relationship between $\lambda_m(T)$ and $\Phi(T)$ for PNdEAm *e*-56f and PNiPAm *i*-46f, one notices that only a tiny decrease by 3-4 nm (10% of the whole range of the shift) in λ_m antecedently occurs before Φ shows an abrupt decrease from T_c (see the top panels of Figures 13 and 14). That is, slight dehydration of the polymer chains is enough to induce the macroscopic phase separation of these systems. We assume that the onset temperature of the abrupt drop in $\lambda_m(T)$ corresponds to the upper limit where only the single chains exist in the solution. Hereinafter, this temperature is named the dehydration point of the polymer chains, T_{dh}.

For PNdEAm *e*-70f and *e*-90f, the relationship between $\lambda_m(T)$ and $\Phi(T)$ is similar to that for PNdEAm *e*-56f. λ_m gradually decreases as *T* goes up until $T=T_{dh}$, and then it shows an exponential change. λ_m keeps decreasing throughout the large temperature range until 70 °C. These results suggest that the exponential decrease in λ_m is not a precursory event for the formation of concentrated droplets, but rather associated with the macroscopic growth of the droplets (or the condensation of polymer chains in the droplets). For PNdEAm, the droplet growth and/or condensation accompanied by the dehydration of polymer chains takes place in a wide temperature range over 30 °C. This result is understandable in the case that the phase boundary of the aqueous PNdEAm solution has a parabola curve because the concentration of the polymer-rich domain increases along the curve. Note that PNdEAm/water system undergoes a typical LLPS.[40]

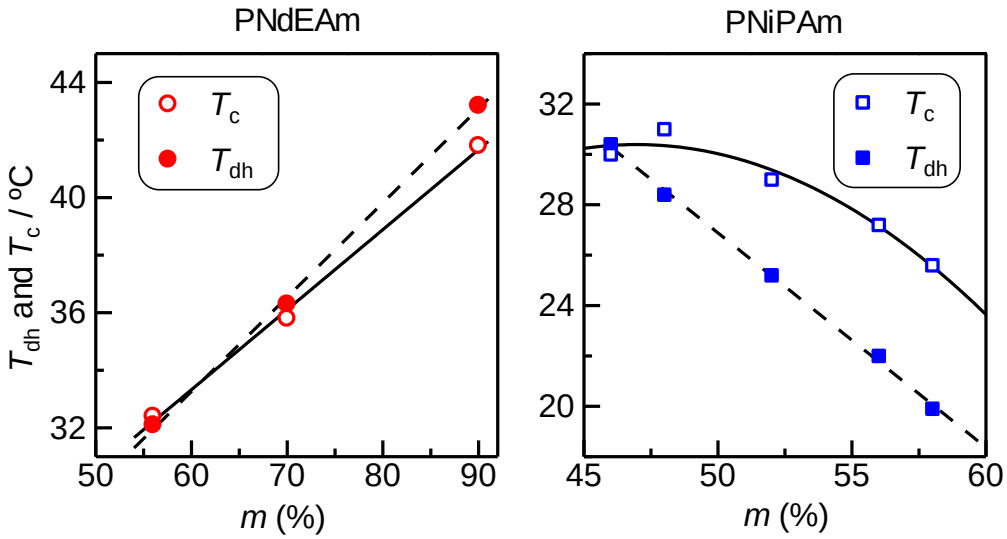

Figure 15. T_C and T_{dh} of the stereo-controlled P(NdEAm-co-DAN) and P(NiPAm-co-DAN) in water at 0.1 wt%.

For PNiPAm *i*-46f, on the other hand, λ_m reaches the lowest value (ca 505 nm) within a narrower temperature range of less than 5 °C. The dehydration of PNiPAm chains is remarkably acute compared with that for PNdEAm. The acute dehydration of PNiPAm chains should be correlated with the characteristic behavior of the droplet growth. Han *et al*. have revealed that the concentrated droplets in the aqueous solution of an atactic PNiPAm (m ~ 46 %) grow only in a limited temperature range between the phase separation temperature and 3.5 °C above.[39] This is in good agreement with the change in $\lambda_m(T)$ for PNiPAm *i*-46f in water. Many researchers have pointed out that the peculiar phase behavior of PNiPAm/water is owing to the cooperative hydration of the polymer chain.[42,43] Since sequential hydration between polymer chains and water molecules is cooperatively in the cooperative hydration, the process becomes highly sensitive to thermal perturbation.

The plots of T_c and T_{dh} against m are shown in Figure 15. For PNdEAm *e*-56f, *e*-70f, *e*-90f, and

PNiPAm *i*-46f, T_c and T_{dh} resemble, while for *m*-rich PNiPAms those are dissociated. The difference between T_{dh} and T_c becomes large with increasing *m*. The *m* dependences of T_c for PNiPAm and PNdEAm are the same as those previously reported.[32,47] The results clearly show that the change in the dehydration of polymer chains is not always interlocked with the macroscopic phase separation of aqueous polymer solutions. For PNiPAms, we infer that there is an intermediate state between T_{dh} and T_c, where the single chains are destabilized but the growth of concentrated droplets is inhibited for some reason. In this region, the droplets remain small, where the incident light of 650 nm may not be scatted sufficiently.

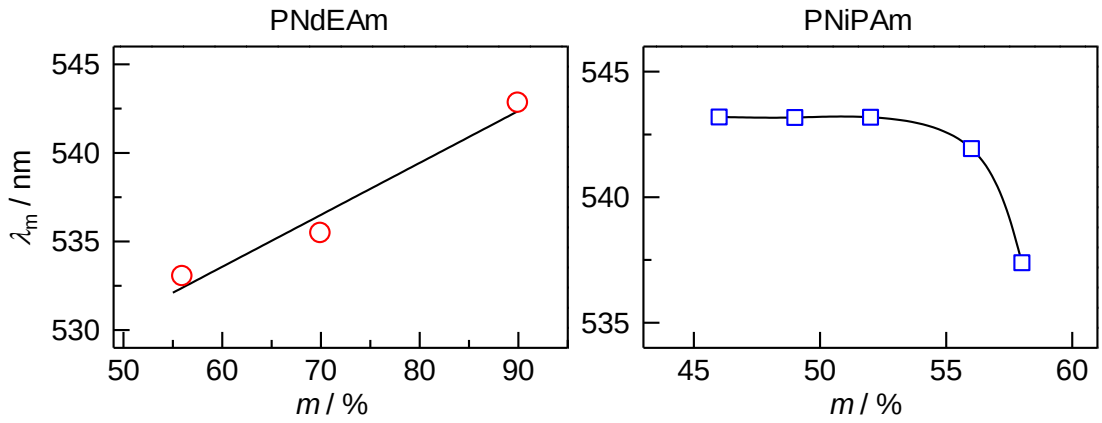

Figure 16. The *m* dependence of λ_m for the stereo-controlled P(NdEAm-co-DAN) and P(NiPAm-co-DAN) in water at 15 °C.

Figure 16 represents λ_m at 15 °C as a function of *m* for P(NdEAm-co-DAN) and P(NiPAm-co-DAN) in water. For PNdEAms, the hydrophobicity (or hydrophilicity) of the chains in a homogeneous phase seems to be correlated with T_c. For PNiPAm, however, the decrease in λ_m for $m \leq 52$ is almost ignorable, while that for $m > 52$ is large. The non-linear dependence of the hydrophobicity of stereo-controlled PNiPAms has also been reported for T_c.[47] Thus, we presume that the hydrophobicity of PNdEAm and PNiPAm is somewhat associated with T_c. In the previous study,

we have revealed that the meso diad configuration is more hydrophobic than the racemo one by ca. 1 kJ mol^{-1}.[54] Molecular mechanics calculation has indicated that the intramolecular interaction of the meso dimer is stronger than that of the racemo one, while the racemo configuration is advantageous in terms of the hydration free energy and conformational entropy. We infer that a similar mechanism is found for the tacticity effects on the hydrophilicity of PNdEAm. Further experimental and theoretical studies are required to reveal it. It should be notified that the comparison between the microenvironment of PNiPAm and PNdEAm chains is not simple; PNdEAm *e*-56f is more hydrophobic (λ_m = 533 nm at 15 °C) than PNiPAm *i*-46f (λ_m = 543 nm at 15 °C) even though T_c of *e*-56f slightly higher than that of *i*-46f. It is therefore inferred that the relationship between the hydration state under the homogeneous phase and T_{dh} changes depending upon the chemical structure of polymers.

Formation and stabilization of nano-order droplets in the intermediate state.

The small angle neutron scattering (SANS) and DLS measurements have revealed that the single chain of PNiPAm with m = 46 – 58 in the 0.2wt% aqueous solution decreases its size monotonically by heating from 10 °C.[55] This may correspond to the gentle decrement of λ_m observed below T_{dh} shown in Figure 14. That is, gradual dehydration causes a continuous shrink of the single chain of PNiPAm. SANS and DLS could not monitor the decreases in the size of single chains above a certain temperature even below T_c, because the contribution of large particles is extremely enhanced in the scattering measurements. As mentioned in the previous section, there is an intermediate state between T_{dh} and T_c, where concentrated droplets grow but the macroscopic LLPS does not proceed. FCS is a powerful tool to detect both the single chain and the aggregate.

We have employed RhB for FCS measurement because the emission wavelength and intensity are stable during the phase change of the aqueous solution of PNiPAm. The difference in the

hydrophobicity of DAN and RhB is expected to be small because the concentration of chromophores in the chain is sufficient low.[46]

Figure 17 shows the FCS autocorrelation function of P(NiPAm-co-RhB) *i*-52r in the 0.1 wt% aqueous solution at 22 and 28 °C. The concentration of the polymer solution was adjusted to 0.1 wt% by mixing fluorescent-labeled *i*-52r and unlabeled *i*-52 to control the number of chromophores for FCS measurements. We have employed RhB for FCS measurement because the emission wavelength and intensity are stable during the phase change of the aqueous solution of PNiPAm. The difference in the hydrophobicity of DAN and RhB is expected to be small because the concentration of chromophores is very low. Several reports have shown that a fluorescence probe does not affect the phase behavior of the aqueous polymer solution.[46]

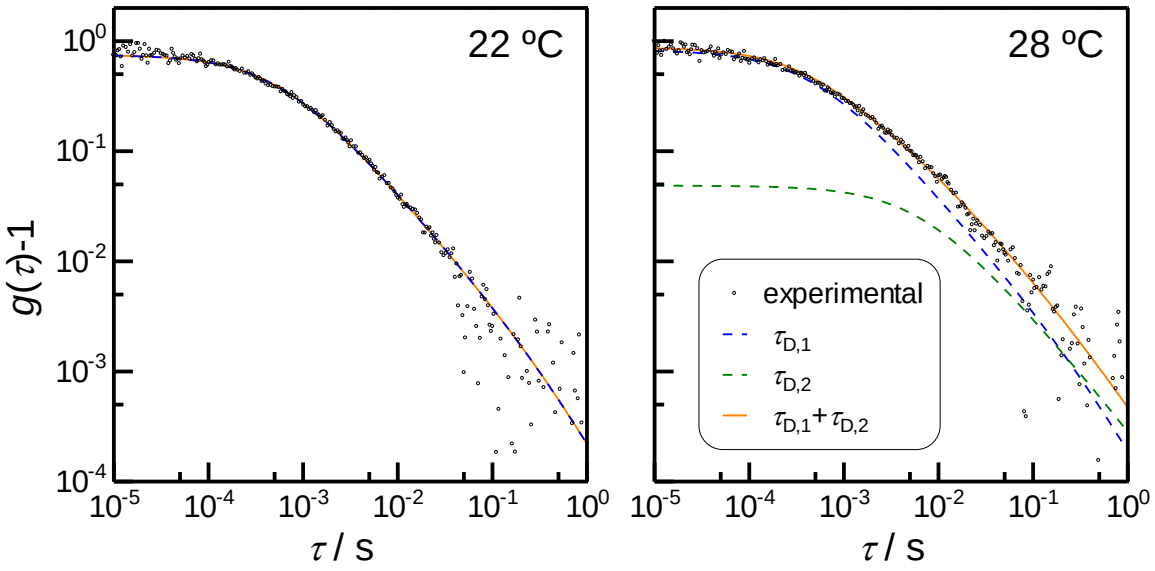

Figure 17. Fitting results of FCS signals for P(NiPAm-co-RhB) *i*-52r in water measured at 0.1 wt%.

The profile at 22 °C can be fitted by a single decay function with $R_h(\tau_{D,1})$ = 3.6 nm using equations (1) and (2) with n=1. The empirical power-law relation between R_h and M_w for atactic PNiPAm in

water gives R_h = 4.8 nm for M_w = 3.9 × 10^4 at 20 °C.[56] Therefore, we infer that *i*-52r in water at 22 °C exists as a single chain. The single decay has been obtained when the temperature is below 24 °C. On the other hand, the FCS autocorrelation function in the temperature range of 24-30 °C contains at least two relaxation modes as shown in the right panel of Figure 17, where $\tau_{D,1}$ and $\tau_{D,2}$ correspond to a fast and slow decay component, respectively. At 28 °C, the ratio of the $\tau_{D,2}$ (slow) component is 0.1, and $R_h(\tau_{D,2})$ is estimated to be *ca*. 45 nm. The temperature dependence on R_h of diffusants is shown in Figure 18. Below 24 °C, PNiPAm *i*-52r exists as a single chain, and then its R_h decreases with increasing temperature. When the temperature closes to T_{dh} (ca. 25 °C), a droplet with *ca*. 45 nm is formed. The size of the droplets does not change from 24 - 28 °C, while their fraction increases from 0.03 to 0.1. Above 29 °C, the reproducibility of the FCS decays becomes worse, because of the existence of large aggregates.

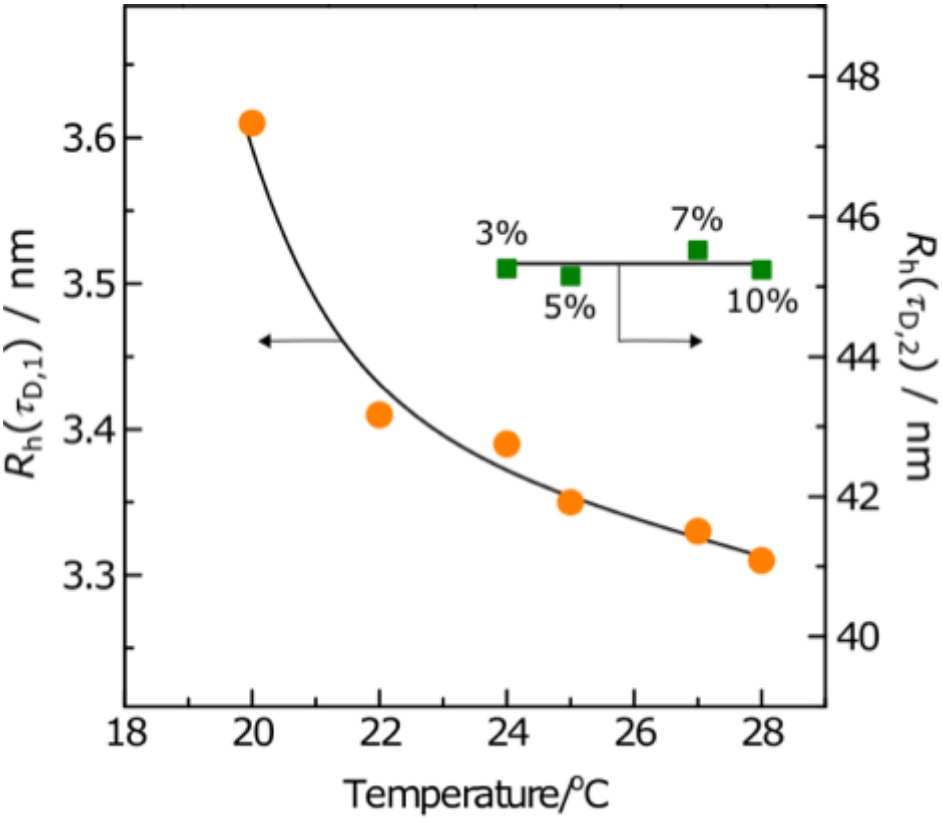

Figure 18. Temperature dependence of R_h values of *i*-52r.

For the aqueous solution of PNiPAm with *m*=52r, the intermediate state is observed between T_{dh} ~ 25 °C and T_c ~ 29 °C as shown in Figure 14. In this temperature range, the FCS results suggest that the droplet with R_h ~ 45 nm increase their fraction without changing the size. There are two possibilities to explain the reason why the fraction of droplets gradually increases but the droplet size remains the same: the distribution in tacticity and molecular weight. If the *m* content of a polymer chain slightly varies, the polymer having a different *m* will be dehydrated at a different temperature. For the molecular weight distribution, a similar thing may occur. Han *et al*. have supposed that the growth inhibition of the concentrated droplets in the aqueous solution of atactic PNiPAm is caused by acute dehydration and condensation.[29] By employing the steady-state fluorescence spectroscopy, we have revealed that the dehydration of PNiPAm occurs in a narrow temperature range. The acute dehydration possibly arises from the secondary amide groups in the side chain of PNiPAm. As we have pointed out previously, the C=O···H–N hydrogen bonding among the side chains may compete with the C=O···H–O hydrogen bonding between the side chain and water, because their interaction energy is similar.[40,41] When the hydrophobic interaction among hydrophobic groups of PNiPAm becomes predominant, the C=O···H–O hydrogen bonds are replaced by the C=O···H–N hydrogen bond, resulting in acute dehydration. The dehydration of the PNdEAm chain occurs gradually because the side chain is a tertiary amide group. There is an additional factor that stabilize the nano-droplets. For the polymerization in the presence of Lewis acid, it has been reported that the *m* content slightly decreases with an increase in conversion, indicating that the product may have a stereo-gradient structure.[57] A hydrophilic part of the stereo-gradient polymers may contribute to the stability of the nano-droplet. It is difficult to consider the nano-droplets as a core-shell micelle because of their size. This may be a minor contribution because the nano-droplet is not stabilized in the aqueous solution of PNdEAm. It is also worth noting that the change in FCS signals shows hysteresis. In the cooling process after the solution is heated up to 30 °C, we can not obtain FCS autocorrelation functions until

below 10 °C. A large hysteresis of λm(T) has also been observed for *m*-rich PNiPAms (Figure S3 in SI), indicating that the nano-droplets are meta-stable.

FCS has shown that the concentrated droplets are formed and stabilized over several temperatures under T_c for the aqueous solution of *m*-rich PNiPAms. Under this situation, the dehydration of the PNiPAm chain proceeds as temperature increases (see in Figure 14.) When the hydrophobicity of PNiPAm chains becomes strong enough in a narrow temperature range, the concentration of droplets reaches so high that the coalescence of the droplets is hindered by the viscoelastic effect.[58] If the rheological relaxation time becomes slower than the characteristic time of the collision because of polymer condensation, the concentrated droplet behaves as an elastic body on the collision time scale. This may cause the stabilization of concentrated droplets in the aqueous solution of *i*-52r. In the diethyl malonate solution of polystyrene, a large temperature jump into the biphasic region is required to observe the viscoelastic effect.[58] For the aqueous solution of PNiPAm, on the other hand, the stabilization of concentrated droplets is observed by a continuous temperature scan. This may be because the acute dehydration of PNiPAm causes an acute condensation of polymers in droplets, resulting in the viscoelastic effects. The result suggests that the acute dehydration of polymer chains plays an important role in the stabilization of nano-order droplets in the vicinity of the macroscopic LLPS. This gives a key to understanding why the small droplets are stabilized in a biological intracellular LLPS.

3.4. Conclusion

In a biological intracellular liquid-liquid phase separation (LLPS), the growth of droplets is often suppressed. In LLPS of synthetic polymers, however, the droplets keep growing until the two distinct phases become observable by the naked eye. To understand the mechanism of how the nano-order droplets are stabilized in a biological intracellular LLPS, we have focused on the characteristic phase behaviors of poly(*N*-isopropylacrylamide) (PNiPAm) in water. To reveal the relationship between the dehydration of polymer chains and the macroscopic LLPS, we have prepared dansyl-labeled PNiPAms with various meso-diad content (*m*). For comparison, dansyl-labeled poly(*N*,*N*-diethylacrylamide) (PNdEAm)s with various *m* are also prepared, because its aqueous solution undergoes a typical phase behavior.

The mean center of the fluorescence for dansyl-labeled polymers (λ_m) gradually decreases below the dehydration temperature T_{dh} corresponding to the onset of the large drop, and then shows an exponential decay. By comparing $\lambda_m(T)$ with the transmittance curve $\Phi(T)$ for atactic PNdEAm and PNiPAm, it is presumed that the droplets arising from LLPS appear just above T_{dh} and the exponential decay of $\lambda_m(T)$ is associated with the dehydration during the growth of droplets. In these cases, the onset of the large drop of $\Phi(T)$, which is referred to as the cloud point (T_c), locates nearby T_{dh}. For *m*-rich PNiPAms, on the other hand, T_{dh} becomes lower than T_c and the difference becomes large with increasing *m*. The result suggests that the change in the dehydration of polymer chains is not always interlocked with the macroscopic phase separation of aqueous polymer solutions.

The λ_m(T) curves reveal that the dehydration of PNiPAm occurs in a much narrow temperature range compared with that of PNdEAm. The sharp dehydration of PNiPAm may cause an acute condensation of polymers in droplets, resulting in the viscoelastic effects that hinder the coalescence of the droplets. Fluorescence correlation spectroscopy (FCS) for PNiPAm with m = 52 % unveils that a droplet having $R_h \sim 45$ nm is formed at around T_{dh} and increases its population until T_c. We

demonstrate that the acute dehydration of polymer chains plays an important role in the stabilization of nano-order droplets in the vicinity of the macroscopic LLPS. This may give a key to understanding the mechanism of the biological intracellular LLPS where small droplets are stabilized.

3.5. Acknowledgments

This work was supported by the Grant-in-Aid for Scientific Research (No. 18K05224) to YK and by Izumi Science and Technology Foundation (2021-J-094) to YS.

3.6. References

(1) Charles M. Schroeder Single polymer dynamics for molecular rheology ; Journal of Rheology 62, 371 (2018)

(2) Elizabeth G. Kelley,wa Julie N. L. Albert,wb Millicent O. Sullivan and Thomas H. Epps, Stimuli-responsive copolymer solution and surface assemblies for biomedical applications Chem. Soc. Rev., 2013, 42, 7057

(3) lgal Szleifer, Polymers and proteins: interactions at interfaces, Solid state and materials science, 1997, 2, 3, 337-344

(4) BruceJ.Berne and Robert Pecora Dynamic Light Scattering with Applications to Chemistry, Biology, and Physics 1976

(5) Parisa Edalati, Yuta Itagoe, Hironori Ishiharac, Tatsumi Ishihara,Hoda Emami, Makoto Arita, Masayoshi Fuji and Kaveh Edalati Visible-light photocatalytic oxygen production on a high-entropy oxide by multiple-heterojunction introduction, Journal of Photochemistry&Photobiology, A: Chemistry 2022,433(1),114167-114181

(6) E. L. Elson and D. Magde, Fluorescence correlation spectroscopy. I. Conceptual basis and theory , Biopolymers 13, 1 (1974).

(7) J. Widengren and R. Rigler, J. Fluoresc. 7, 211 (1996).

(8) Watt W. Webb Fluorescence correlation spectroscopy : inception, biophysical experimentations , and prospectus APPLIED OPTICS 40, 24,3969-3983

(9) MagdeD,ElsonEL,WebbWW.1972.Thermodynamic fluctuations in a reactingsystem: measurement by fluorescence correlation spectroscopy. Phys. Rev. Lett. 29:705–8

(10) Dominik Wo¨ll Fluorescence correlation spectroscopy in polymer science RSC Adv., 2014, 4, 2447–2465

(11) A. Michelman-Ribeiro, H. Boukari, R. Nossal andF. Horkay, Macromolecules, 2004, 37, 10212–10214.

(12) Piletsky S.; Turner A.: in Molecular Imprinting of Polymers. Landes-Bioscience, Georgetown, 2006.

(13) Turiel E., Martin-Esteban A.: Anal. Chim. Acta 668, 87 (2010).

(14) R.Rigler and E.S.Elson Fluorescence Correlation Spectroscopy Theory and Applications 2001

(15) Müller, C. B.; Loman, A.; Pacheco, V.; Koberling, F.; Willbold, D.; Richtering, W.; Enderlein, J. Precise Measurement of Diffusion by Multi-Color Dual-Focus Fluorescence Correlation Spectroscopy. EPL (Europhysics Lett. 2008, 83 (4), 46001

(16) Shiraki, K. Soubunri Seibutsugaku (Phasing Biology); Tokyo Kagaku-Doujin: Tokyo, 2019.

(17) Kamimura, Y. R.; Kanai, M. Chemical Insights into Liquid-Liquid Phase Separation in Molecular Biology. Bull. Chem. Soc. Jpn. 2021, 94 (3), 1045–1058.

(18) Alberti, S.; Gladfelter, A.; Mittag, T. Considerations and Challenges in Studying Liquid-Liquid Phase Separation and Biomolecular Condensates. Cell. Cell Press January 24, 2019, pp 419–434.

(19) Molliex, A.; Temirov, J.; Lee, J.; Coughlin, M.; Kanagaraj, A. P.; Kim, H. J.; Mittag, T.; Taylor, J. P. Phase Separation by Low Complexity Domains Promotes Stress Granule Assembly and Drives Pathological Fibrillization. Cell 2015, 163 (1), 123–133.

(20) Murthy, A. C.; Dignon, G. L.; Kan, Y.; Zerze, G. H.; Parekh, S. H.; Mittal, J.; Fawzi, N. L. Molecular Interactions Underlying Liquid－liquid Phase Separation of the FUS Low-Complexity Domain. Nat. Struct. Mol. Biol. 2019, 26 (7), 637–648.

(21) Snead, W. T.; Gladfelter, A. S. The Control Centers of Biomolecular Phase Separation: How Membrane Surfaces, PTMs, and Active Processes Regulate Condensation. Molecular Cell. Cell Press October 17, 2019, pp 295–305.

(22) Pak, C. W.; Kosno, M.; Holehouse, A. S.; Padrick, S. B.; Mittal, A.; Ali, R.; Yunus, A. A.; Liu, D. R.; Pappu, R. V.; Rosen, M. K. Sequence Determinants of Intracellular Phase Separation by Complex Coacervation of a Disordered Protein. Mol. Cell 2016, 63 (1), 72–85.

(23) Qamar, S.; Wang, G. Z.; Randle, S. J.; Ruggeri, F. S.; Varela, J. A.; Lin, J. Q.; Phillips, E. C.; Miyashita, A.; Williams, D.; Ströhl, F.; et al. FUS Phase Separation Is Modulated by a Molecular Chaperone and Methylation of Arginine Cation-π Interactions. Cell 2018, 173 (3), 720-734.e15.

(24) Peng, A.; Weber, S. C. Evidence for and against Liquid-Liquid Phase Separation in the Nucleus. Non-Coding RNA 2019, Vol. 5, Page 50 2019, 5 (4), 50.

(25) Watanabe, R.; Takaseki, K.; Katsumata, M.; Matsushita, D.; Ida, D.; Osa, M. Characterization of Poly(N,N-Diethylacrylamide) and Cloud Points in Its Aqueous Solutions. Polym. J. 2016, 48 (5), 621–628.

(26) Matsuda, Y.; Miyazaki, Y.; Sugihara, S.; Aoshima, S.; Saito, K.; Sato, T. Phase Separation Behavior of Aqueous Solutions of a Thermoresponsive Polymer. J. Polym. Sci. Part B Polym. Phys. 2005, 43 (20), 2937–2949.

(27) Tong, Z.; Zeng, F.; Zheng, X.; Sato, T. Inverse Molecular Weight Dependence of Cloud Points for Aqueous Poly(N-Isopropylacrylamide) Solutions. Macromolecules 1999, 32 (13), 4488–4490.

(28) Maeda, Y.; Yamamoto, H.; Ikeda, I. Phase Separation of Aqueous Solutions of Poly(N-Isopropylacrylamide) Investigated by Confocal Raman Microscopy. Macromolecules 2003, 36 (14), 5055–5057.

(29) Han, J.; Takahashi, R.; Kuang, C.; Sato, T. Phase Separation Behavior of Aqueous Poly(N-Isopropylacrylamide) Solutions Studied by Scattering Experiments. Langmuir 2022, 38 (17),5089–5097.

(30) Chan, K.; Pelton, R.; Zhang, J. On the Formation of Colloidally Dispersed Phase-Separated Poly(N-Isopropylacrylamide). Langmuir 1999, 15 (11), 4018–4020.

(31) Gorelov, A. V.; Du Chesne, A.; Dawson, K. A. Phase Separation in Dilute Solutions of Poly (N-Isopropylacrylamide). Phys. A Stat. Mech. its Appl. 1997, 240 (3–4), 443–452.

(32) Katsumoto, Y.; Kubosaki, N. Tacticity Effects on the Phase Diagram for Poly(<italic>N</Italic>-Isopropylacrylamide) in Water. Macromolecules 41 (15), 5955–5956.

(33) Katsumoto, Y.; Etoh, Y.; Shimoda, N. Phase Diagrams of Stereocontrolled Poly(<italic>N</Italic>,<italic>N</Italic>-Diethylacrylamide) in Water. Macromolecules 43 (6), 3120–3121.

(34) Freitag, R.; Garret-Flaudy, F. Salt Effects on the Thermoprecipitation of Poly(N-Isopropylacrylamide) Oligomers from Aqueous Solution. Langmuir 2002, 18 (9), 3434–3440.

(35) Idziak, I.; Avoce, D.; Lessard, D.; Gravel, D.; Zhu, X. X. Thermosensitivity of Aqueous Solutions of Poly(N,N-Diethylacrylamide). Macromolecules 1999, 32 (4), 1260–1263.

(36) Winnik, F. M.; Ringsdorf, H.; Venzmer, J. Methanol-Water as a Co-Nonsolvent System for Poly(N-Isopropylacrylamide). Macromolecules. May 1, 1990, pp 2415–2416.

(37) Maeda, Y.; Nakamura, T.; Ikeda, I. Change in Solvation of Poly(N,N-Diethylacrylamide) during Phase Transition in Aqueous Solutions as Observed by IR Spectroscopy. Macromolecules 2002, 35 (27), 10172–10177.

(38) Hamamura, K.; Watanabe, K.; Sanada, Y.; Tanaka, F.; Katsumoto, Y. Relationship between the Phase Diagram and Hysteresis in Demixing and Remixing for Atactic and Meso-Rich Poly(N-Isopropylacrylamide)s in Water. Polymer (Guildf). 2019, 16192–100.

(39) Cheng, H.; Shen, L.; Wu, C. LLS and FTIR Studies on the Hysteresis in Association and Dissociation of Poly(N-Isopropylacrylamide) Chains in Water. Macromolecules 2006, 39 (6), 2325–2329.

(40) Katsumoto, Y.; Tanaka, T.; Sato, H.; Ozaki, Y. Conformational Change of Poly(N-Isopropylacrylamide) during the Coil-Globule Transition Investigated by Attenuated Total Reflection/Infrared Spectroscopy and Density Functional Theory Calculation. J. Phys. Chem. A 2002, 106 (14), 3429–3435.

(41) Katsumoto, Y.; Tanaka, T.; Ihara, K.; Koyama, M.; Ozaki, Y. Contribution of Intramolecular C<private-Char><inline-Graphic Href="dbd.Gif" Mimetype="image" Type="simple" Medium="dbd.Gif"></Inline-Graphic></Private-Char>O···H－N Hydrogen Bonding to the Solvent-Induced Reentrant Phase Separation of Poly(<italic>N</Italic>-Isopropylacrylamide). J. Phys. Chem. B 111 (44), 12730–12737.

(42) Kawaguchi, T.; Kobayashi, K.; Osa, M.; Yoshizaki, T. Is a Cloud-Point Curve in Aqueous Poly(N-Isopropylacrylamide) Solution Binodal? J. Phys. Chem. B 2009, 113 (16), 5440–5447.

(43) Hamamura, K.; Watanabe, K.; Sanada, Y.; Tanaka, F.; Katsumoto, Y. Relationship between the Phase Diagram and Hysteresis in Demixing and Remixing for Atactic and Meso-Rich Poly(N-Isopropylacrylamide)s in Water. Polymer (Guildf). 2019, 161, 92–100.

(44) Tanaka, F.; Katsumoto, Y.; Nakano, S.; Kita, R. LCST Phase Separation and Thermoreversible Gelation in Aqueous Solutions of Stereo-Controlled Poly(N-Isopropylacrylamide)S. React. Funct. Polym. 2013, 73 (7), 894–897.

(45) Shea, K. J.; Stoddard, G. J.; Shavelle, D. M.; Wakui, F.; Choate, R. M. Synthesis and Characterization of Highly Cross-Linked Polyacrylamides and Polymethacrylamides. A New Class of Macroporous Polyamides. Macromolecules 1990, 23 (21), 4497–4507.

(46) Asano, M.; Winnik, F. M.; Yamashita, T.; Horie, K. Fluorescence Studies of Dansyl-Labeled Poly(N-Isopropylacrylamide) Gels and Polymers in Mixed Water/Methanol Solutions. Macromolecules 1995, 28 (17), 5861–5866.

(47) Ray, B.; Okamoto, Y.; Kamigaito, M.; Sawamoto, M.; Seno, K.; Kanaoka, S.; Aoshima, S. Effect of Tacticity of Poly(N-Isopropylacrylamide) on the Phase Separation Temperature of Its Aqueous Solutions. Polym. J. 2005, 37 (3), 234–237.

(48) Katsumoto, Y.; Kubosaki, N. Tacticity Effects on the Phase Diagram for Poly(N-Isopropylacrylamide) in Water. Macromolecules 2008, 41 (15), 5955–5956.

(49) Katsumoto, Y.; Etoh, Y.; Shimoda, N. Phase Diagrams of Stereocontrolled Poly(N,N-Diethylacrylamide) in Water. Macromolecules 2010, 43 (6) , 3120–3121.

(50) Sahoo, B.; Sil, T. B.; Karmakar, B.; Garai, K. A Fluorescence Correlation Spectrometer for Measurements in Cuvettes. A Fluoresc. Correl. Spectrom. Meas. Cuvettes 2018, 115 (3), 445–466.

(51) Müller, C. B.; Loman, A.; Pacheco, V.; Koberling, F.; Willbold, D.; Richtering, W.; Enderlein, J. Precise Measurement of Diffusion by Multi-Color Dual-Focus Fluorescence Correlation Spectroscopy. EPL (Europhysics Lett. 2008, 83 (4), 46001.

(52) Schild, H. G.; Tirrell, D. A. Microcalorimetric Detection of Lower Critical Solution Temperatures in Aqueous Polymer Solutions. J. Phys. Chem. 1990, 94 (10), 4352–4356.

(53) Okada, Y.; Tanaka, F. Cooperative Hydration, Chain Collapse, and Flat LCST Behavior in Aqueous Poly(N-Isopropylacrylamide) Solutions. Macromolecules 2005, 38 (10), 4465–4471.

(54) Katsumoto, Y.; Kubosaki, N.; Miyata, T. Molecular Approach to Understand the Tacticity Effects on the Hydrophilicity of Poly(N-Isopropylacrylamide): Solubility of Dimer Model Compounds in Water. J. Phys. Chem. B 2010, 114 (42), 13312–13318.

(55) Nishi, K.; Hiroi, T.; Hashimoto, K.; Fujii, K.; Han, Y.-S.; Kim, T.-H.; Katsumoto, Y.; Shibayama, M. SANS and Dls Study of Tacticity Effects on Hydrophobicity and Phase Separation of Poly(N -Isopropylacrylamide). Macromolecules 2013, 46 (15), 6225–6232.

(56) Kubota, K.; Fujishige, S.; Ando, I. Solution Properties of Poly(N-Isopropylacrylamide) in Water. Polym. J. 1990, 22 (1), 15–20.

(57) Ray, B.; Isobe, Y.; Matsumoto, K.; Habaue, S.; Okamoto, Y.; Kamigaito, M.; Sawamoto, M. RAFT Polymerization of N-Isopropylacrylamide in the Absence and Presence of Y(OTf)3: Simultaneous Control of Molecular Weight and Tacticity. Macromolecules 2004, 37 (5), 1702–1710.

(58) Tanaka, H. Unusual Phase Separation in a Polymer Solution Caused by Asymmetric Molecular Dynamics. Phys. Rev. Lett. 1993, 71 (19), 3158.

Chapter 4: Supporting information

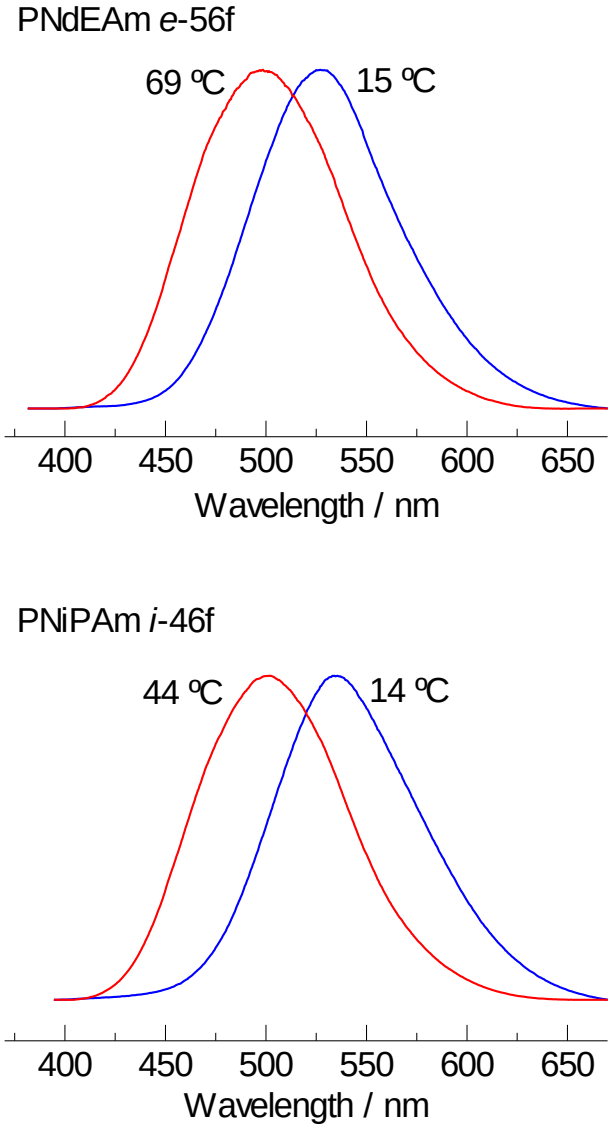

Figure S1. Fluorescence emission spectra of PNdEAm *e*-56f and PNiPAm *i*-46f measured below and above T_c.

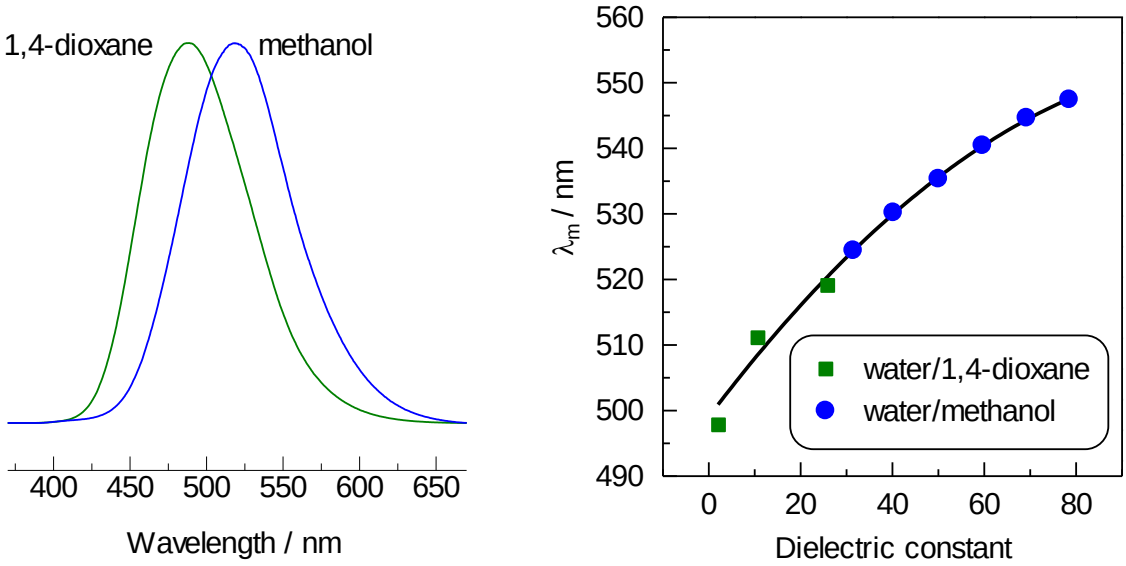

Figure S2. (Right) Fluorescence emission spectra of DAN monomer in 1,4-dioxane and in methanol at 25 °C. (Left) Shifts in λ_m of DAN monomer in water/methanol and water/1.4-dioxane mixture. The dielectric constant ε_r of water, methanol, and 1.4-dioxane is 80.1, 32.7, and 2.25, respectively.

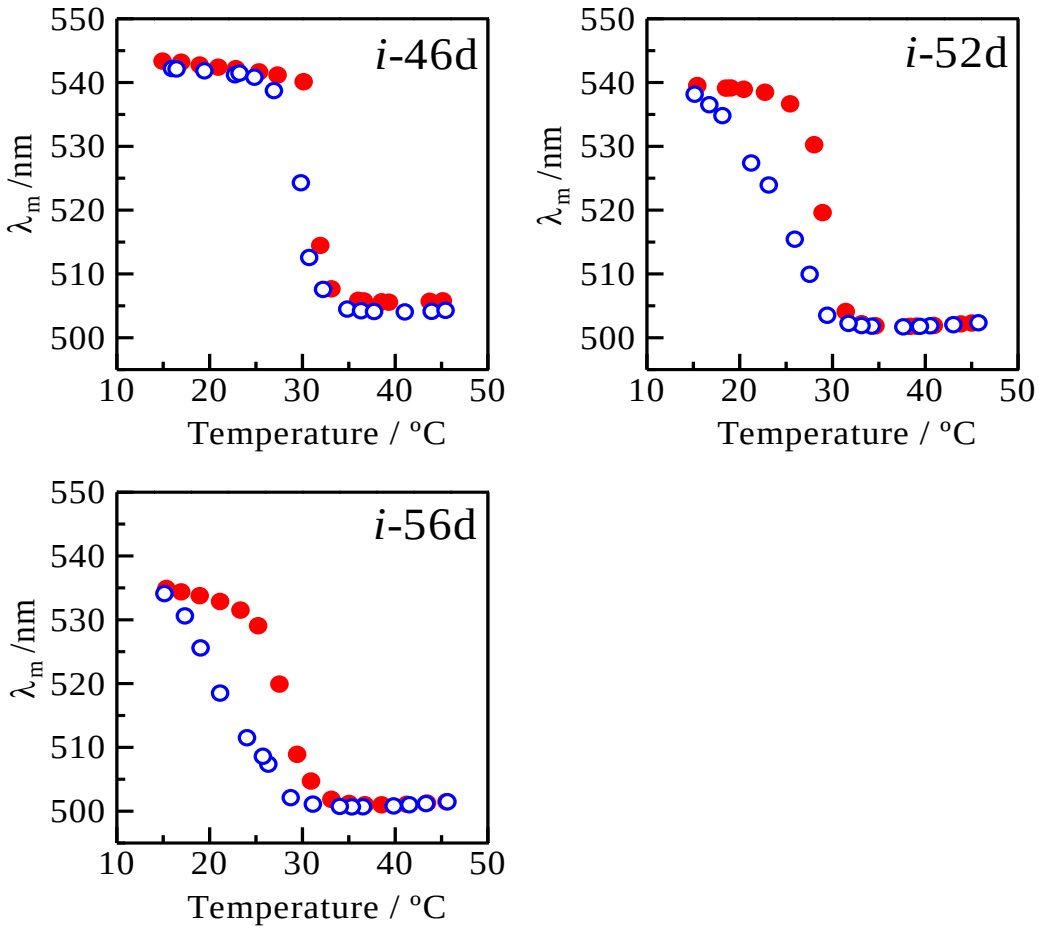

Fig. 3. Hysteresis of $\lambda_m(T)$ for the 0.1 wt% aqueous solutions of *m*-rich PNiPAms: the heating process (red closed circles) and the cooling process (blue open circles).